A Geometrical Solution to the Sharkskin Instability†

Harshawardhan V. Pol,‡ Yogesh M. Joshi,*,§ Prashant S. Tapadia,‡,⊥ Ashish K. Lele,‡ and Raghunath A. Mashelkar*,#

Polymer Science and Engineering Division, National Chemical Laboratory, Pune 411008, India, Department of Chemical Engineering, Indian Institute of Technology, Kanpur, Kanpur 208016, India, and Council of Scientific and Industrial Research, Anusandhan Bhavan, 2 Rafi Marg, New Delhi 110001, India

We study the effect of die exit divergence on the sharkskin behavior, both experimentally as well as through the use of computational fluid dynamics (CFD) simulations. Sharkskin or surface fracture is known to occur immediately after the die exit, because of the large elongational deformation that a polymer melt experiences as it exits the die. We show that the diverging taper at the die exit postpones or completely removes the occurrence of sharkskin. The corresponding CFD simulations of an equivalent K−BKZ fluid show that the taper at the die exit significantly reduces the severity of the elongational flow, thereby reducing the normal stresses as the polymer melt leaves the die. We believe that, in an extrusion operation, the provision of a diverging taper at the die exit is one of the potential measures by which sharkskin instability can be eliminated on an industrial scale.

I. Introduction

The sharkskin instability has important implications on polymer extrusion processes. In particular, it limits the processing speed to a critical value above which the quality of the extruded products may suffer adversely. Because of its industrial relevance, the sharkskin instability has been explored extensively over the past six decades. The main motivation behind such studies is to understand the mechanisms, both at macroscopic and microscopic levels, that are underlying this phenomenon and to suggest strategies to eliminate the sharkskin instability.

Generally three types of extrudate distortions are observed while performing the extrusion of a polymer melt.[1,2] At lower shear rates, ripples perpendicular to the flow direction are observed on the surface of the extrudate. This behavior is observed irrespective of the mode of operation (either pressure-controlled or flow-rate-controlled). Such ripples are popularly known as sharkskin or are sometimes called surface fracture. The second type of distortion occurs only in the rate-controlled mode, when periodic pressure and flow-rate oscillations are observed. The emerging extrudate seems to be bamboolike, where periodic rough and smooth bands on the surface can be observed.[3] The third type of distortion is manifested as a gross distortion of the extrudate or smooth spirals. This instability is known to originate at the die entrance and is also known as entry instability.[4] The intensity and/or presence of any of the aforementioned instabilities are dependent on the various characteristics of the polymer melt, as well as its interactions with the die wall. In this paper, we will limit ourselves only to sharkskin instability.

We suggest that a diverging taper at the die exit significantly attenuates the sharkskin instability. We study this behavior through experiments as well as numerical simulations. This paper is designed as follows: In the background section, we present an overview of the literature particularly with regard to mechanism of sharkskin. In section III, we describe the experimental procedure. This contains the details of the extrusion experiments with dies that have divergent exits and other rheological characterization (section IV) that is needed to support the numerical simulations. In section V, we present the numerical scheme, followed by an analysis of the observed phenomenon.

II. Background

The first experimental observation of surface defects during extrusion apparently dates back to 1942. Garvey and co-workers[5] observed extrudate distortion while extruding a synthetic rubber compound through a tire thread die at 110 °C. After this early observation, several research groups investigated the phenomenon in various other polymers. Many terms have been used in the literature (as mentioned in the review of Boudreaux and Cuculo[6]) to describe extrudate distortion, namely melt fracture, elastic turbulence, waviness, ripples, sharkskin, etc. The various details of sharkskin distortion phenomenon, as investigated by several research groups, have been reviewed extensively.[1,4,6−12] In this section, we will summarize only some of the key observations.

Sharkskin or surface fracture is the first indication of instability, and it occurs at a comparatively lower shear stress. In the early days of research in this area, gross distortion of the extrudate surface was often confused with sharkskin behavior. Benbow and Lamb[13] demonstrated the distinct differences between the gross fracture and sharkskin. Although gross distortions occur as a result of melt fracture due to entry instability, sharkskin distortions are localized only at the surface of an extrudate and are also called surface instabilities. Piau et al.[14] defined sharkskin as a surface defect characterized by a small scale and high-frequency rugosity of the free surface that was due to the relaxation of strain at the die outlet. Generally, sharkskin is observed in polymers such as high-density polyethylene (HDPE),[15] linear low-density polyethylene

† Dedicated to Professor M. M. Sharma on the occasion of his 70th birthday.

* To whom correspondence should be addressed. For YMJ: Tel., 91-512-2597993; Fax, 91-11-2590104; E-mail address: joshi@iitk.ac.in. For RAM: Tel., 91-11-23710472; Fax, 91-11-23710618; E-mail address: dgcsir@csir.res.in.

‡ Polymer Science and Engineering Division, National Chemical Laboratory.

§ Department of Chemical Engineering, Indian Institute of Technology.

⊥ Current Address: Department of Polymer Science, University of Akron, Akron, OH 44325-3909.

Council of Scientific and Industrial Research, Anusandhan Bhavan.

10.1021/ie0610391 CCC: $37.00
Published on Web 11/08/2006

(LLDPE),[16,17] polybutadine,[18] polypropylene (PP),[19] polydimethylsiloxane (PDMS),[14] etc. whereas other polymers directly show either stick slip transition or gross distortion (or spirals), without showing sharkskin.

In most cases, it has been determined that coating the die surface with a fluoropolymer can eliminate the sharkskin effect.[20−25] However, in some cases, sharkskin is observed to persist, even after the die has been coated with a fluoropolymer.[26,27] Instead of coating the entire die, Moynihan et al.[20] coated only the entry and the exit regions of the slit die independently and observed the suppression of sharkskin in both cases. Similar observations on the elimination of sharkskin due to die lip (exit) coating have been made by others.[23,25] Sornberger et al.[28] observed that sharkskin appears at a critical value of shear rate, and this critical shear rate increases as the temperature increases. They further observed that mixing a lubricant with LLDPE attenuates the severity of the sharkskin. Nam,[29] as well as Rudin et al.,[30] have also observed the reduction of sharkskin by mixing lubricants or fluoropolymers in the polymer melt. Migler et al.[31] used a capillary rheo-optics technique to understand the mechanism of elimination of sharkskin when a fluoropolymer is added. They observed that the fluoropolymer migrates to the capillary wall, where it sticks and induces slippage between itself and LLDPE, which leads to the elimination of sharkskin. Migler and co-workers[32] further observed that fluoropolymer droplets first adsorb in the entrance region of the die and migrate under shear stress toward the capillary exit, where they act to suppress sharkskin. They observed that a uniform coating in the range of 25−60 nm is sufficient for sharkskin elimination. Hatzikiriakos et al.[33] studied the addition of boron nitride on the melt fracture behavior of polyolefins and observed the elimination of sharkskin. Very recently, Hatzikiriakos and co-workers[34] proposed that boron nitride behaves as an energy dissipater that suppresses the rapid increase of elongational stress.

Howells and Benbow[35] proposed that, as the radius of the capillary die is varied, the sharkskin occurs at the same velocity of the extrudate. Moynihan et al.[20] also varied the length-to-diameter ratio (L/D) of the capillary and observed that the sharkskin was delayed and occurred at higher shear rates with an increase in L/D. Similar behavior has also been observed by Sornberger et al.[28] Although Moynihan et al.[20] and Sornberger et al.[28] observed a substantial influence of die geometry on sharkskin, Venet and Vergnes,[36] Constantin,[37] and Beaufils et al.[38] reported only a weak dependence of sharkskin on L/D. Kurtz[39] was the first to observe a distinct change in the slope of the shear rate−shear stress flow curve at the onset of sharkskin. Ramamurthy,[40] Kalika and Denn,[41] and Wang et al.[25] have also made similar observations for LLDPE at various temperatures. Wang et al.[25] also used a die with 60° diverging exit taper. The effect of this less-abrupt exit leads to a smaller slope change. Generally, although a change in slope of the flow curve is visible at the onset of sharkskin, it is not as severe as that observed during the stick slip instability regime at higher stress.

Molecular structure significantly affects the sharkskin behavior. Not all polymers, which show stick-slip behavior, show sharkskin and vise versa. As discussed earlier, sharkskin is mainly observed in polyolefins and PDMS. Among polyolefins, sharkskin is commonly observed in polymers with a linear chain structure, such as HDPE and LLDPE. Commercial LDPE, which has long branches and high polydispersity, does not show sharkskin.[25,36,42] Contrary to this, Mackley et al.[43] observed surface instability for LDPE at a low temperature of ∼140 °C. However, the same vanished at higher temperatures. It is generally observed that the lower the polydispersity, the higher the severity of sharkskin.[10] Kazatchkov and co-workers[44] studied various LLDPEs with the same weight-average molecular weight and different polydispersities. They observed that the apparent shear rate at the onset of sharkskin increases with polydispersity. After a critical polydispersity of ∼9.6, sharkskin vanished and spirally distorted extrudate appeared out of the die. Hatzikiriakos et al.[45] observed an absence of sharkskin while extruding single-site-catalyzed metallocene LLDPE. They argued that, although these metallocene LLDPE are less polydisperse, they have higher long-chain branching than conventional LLDPE. However, contrary to this observation, Deeprasertkul et al.[16] observed the sharkskin for metallocene LLDPE. Stereoregularity is also shown to be influencing the sharkskin behavior. Tapadia et al.[19] observed sharkskin in syndiotactic PP, whereas, for isotactic PP, sharkskin was completely absent. They argued that lower entanglement molecular weight of syndiotactic PP makes it prone to undergo sharkskin instability.

Venet and Vergnes[36] claimed that, because LDPE has a strong strain-hardening elongational behavior (i.e., higher melt strength), it is resistant to rupture and, hence, does not show sharkskin. Rutgers et al.[46] supported the argument of random crack formation under the influence of high tensile stress at the die exit by analyzing the flow field by means of optical stress birefringence. Rutgers and Mackley,[47] through numerical simulations and experiments on two grades of LLDPE, showed that the onset of the surface fracture (exit tensile stress) correlated well with the critical stress level for melt rupture. Venet and Vergnes[48] have also performed a numerical study of the flow conditions at the die exit. They observed the existence of a small traction zone located at the periphery of the die exit, where the tensile stress grows as the flow rate increases. They further observed that the intensity and the dimensions of the traction zone remain unaffected, because of die geometry. Based on these observations, they argue that the tangential stress cannot be a unique parameter to explain the sharkskin phenomena and the history of deformation should also be taken into account. Moynihan et al.[20] argued that the first requirement for surface melt fracture to occur is that the material be pre-stressed, and the second requirement is the acceleration of the melt as it exits the die.

Various mechanisms have been proposed to explain this behavior. Benbow and Lamb[13] argued that sharkskin is initiated at the die exit. Vinogradov et al.,[49] based on birefringence studies, argued that the high stresses at the die exit cause the sharkskin-like surface distortion. In a seminal paper, Cogswell[50] proposed that the stress singularity near the die exit could cause the local stress to exceed the melt strength of the polymer. This causes rupture of the polymer melt, which results in the sharkskin. Ramamurthy[40] and Kalika and Denn[41] reported that the origin of the sharkskin is due to the loss of adhesion between the polymer and the die wall. Dhori et al.[51] proposed a molecular mechanism, in which they attributed the sharkskin to the wetting−dewetting (adsorption−desorption of the polymer molecules) process at the die lip (exit). Barone and co-workers[52] argued that, because of higher exit stresses and/or elongational flow component near the die exit, the molecules tethered in the die lip region undergo a reversible transition from a coil (entangled state) to stretch (disentangled state) much earlier than those in the die land. This results in cycles of local stress relaxation and growth, which produces a periodic perturbation of the extrudate swell that appears similar to sharkskin roughening on the extrudate surface. They estimated the sharkskin

Table 1. Linear Viscoelastic Relaxation Spectrum (G_i,λ_i) for Elite 5401 at 190 °C

mode	λ_i (s)	G_i (Pa)
1	0.0039	236250
2	0.0300	50402
3	0.0833	13706
4	0.2315	6624.4
5	0.6431	1662.5
6	1.7865	490.32
7	4.9627	225.98
8	13.786	31.701

frequency, using the average distance between two ripples and the velocity of the cooled extrudate, and determined that it follows a WLF-like temperature dependence in a manner similar to that exhibited by the melt viscosity (or the molecular relaxation time). Wang et al.[25] showed that the frequency of sharkskin correlates well with the characteristic molecular relaxation time determined by linear viscoelastic measurements. They argued that this observation correlates the sharkskin to a molecular relaxation process that is triggered by a reversible coil-to-stretch transition. Barone and Wang[53] conducted rheo-optical experiments to show that the presence of tethered chains in the die exit region is a necessary criterion for generating the sharkskin on the extrudate. They wetted the die exit using ethanol to ensure no adsorption of polymer chains in the die lip region. They observed the extrudate to be smooth, even when the stress levels obtained by birefringence substantially exceeded the onset value for sharkskin formation for a bare die.

Migler et al.[31] studied the flow kinetics of a polyethylene extruded through the exit using high-speed video microscopy and observed two distinct material failures during each sharkskin cycle; the first is cohesive and splits the material into two regions, and the second occurs at the polymer/wall interface. They argued that the elongational rate at the die exit is not the discerning criterion to observe sharkskin. They proposed that, because a finite time is required to build a given level of extensional stress in a polymer, the time of application of deformation, as well as the deformation rate, are both important. From a simple analysis of their experimental data, they suggested that sharkskin would occur beyond a critical value of the "reconfiguration rate", which is a product of the elongational rate and the relative deformation in the vicinity of die exit. This criterion explained the observation of sharkskin in polyethylene with and without fluoropolymer.[12,27,54] Recently, Joshi and Denn[55−57] proposed a scaling model to predict the rupture behavior of an entangled polymer melt in an elongational flow. They proposed that catastrophic failure occurs when the friction force on an entangled chain can no longer balance the tension in the chain. They argued that the sharkskin instability is due to rupture of the polymer melt when subjected to elongational flow, which results in tensile stress concentration at the point of departure of the melt from the die.

III. Experimental Section

The LLDPE resin investigated in this work (Elite 5401, The Dow Chemical Company, Midland, MI) was characterized for its melt viscoelastic properties under shear and elongation deformations. The weight-average molecular weight of this material is 104.2 kg/g-mol, whereas its polydispersity index is 2.67. The linear viscoelastic characteristics were measured using oscillatory shear experiments that were performed on an ARES rheometer. The linear viscoelastic relaxation spectrum is shown in Table 1. The nonlinear properties in shear mode were measured by performing steady high-shear experiments using

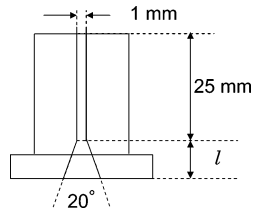

Figure 1. Schematic of the brass die used for carrying out the experiments.

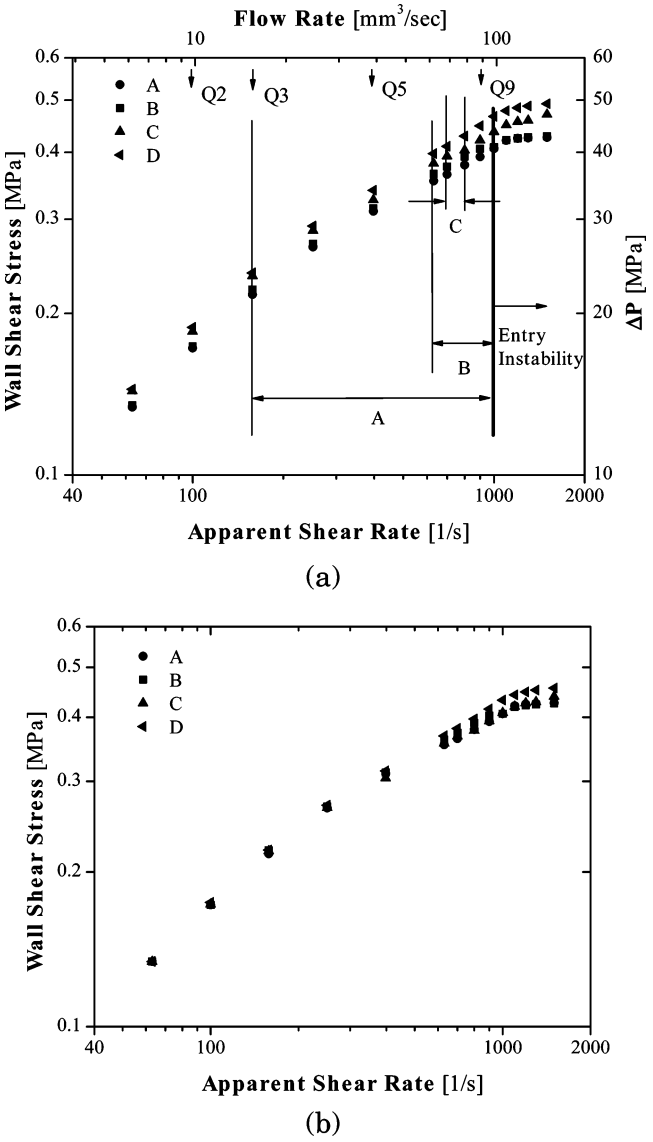

Figure 2. (a) Experimental capillary pressure drop−volumetric flow rate for all capillary dies at 190 °C; the vertical lines show the range of flow rates for which sharkskin was observed for flow through the respective die. (b) Manual shifting of steady high-shear capillary data to determine the equivalent capillary lengths for shear stress−shear rate data at 190 °C.

Table 2. Diverging Die Length of Various Dies Used as Shown in Figure 1

	die A	die B	die C	die D
diverging die length, l	0	3	5	8

a rate-controlled capillary rheometer (CEAST, Model Rheovis 2100), whereas the transient uniaxial extensional behavior was mapped using a commercially available extensional rheological accessory (SER, Xpansion Instruments Inc., USA) that was fitted to an ARES rheometer.

Extrusion experiments were conducted using the capillary rheometer at a temperature of 190 °C. LLDPE was extruded

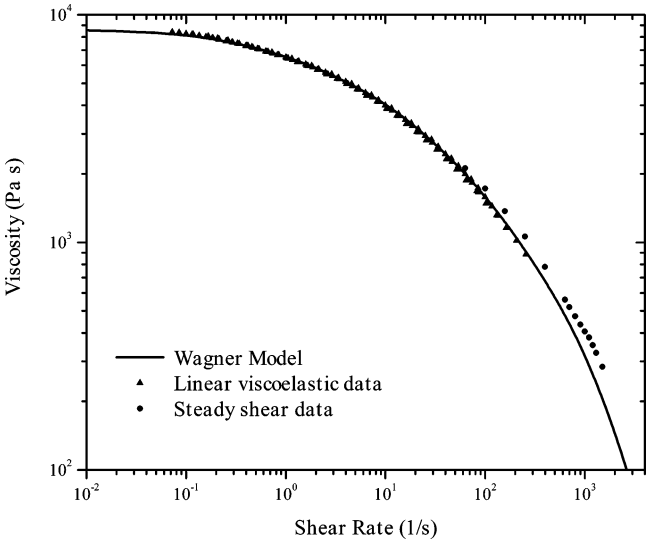

Figure 3. KBKZ model (containing a Wagner irreversible damping function) fit to simple shear data at 190 °C.

through four different brass dies that had a capillary diameter of 1.0 mm, an L/D value of 25 for the die land, and different lengths of the divergence section. Figure 1 shows the schematic of a capillary die, and Table 2 gives various specific details of the each die. Figure 2a displays the experimental (steady high-shear) pressure drop−volumetric flow rate data for all the capillary dies used in this study. The corresponding wall shear stress−apparent shear rate $((r/2)(\Delta P/\Delta L)-4Q/(\pi r^3))$ axes on the same plot have been evaluated by considering only the length of the straight section of the capillaries, which is 25 mm. The range of flow rates for which sharkskin was observed for each die is indicated on the plot. It can be observed that, as the length of the divergent section increased, the range of flow rates over which sharkskin was observed decreased significantly. For the capillary that had a divergent exit length of 8 mm, sharkskin was not observed at any flow rate. Furthermore, a completely distorted extrudate was observed at the same flow rate for all dies, irrespective of the length of their divergent sections. This behavior may be expected, because the origin of this gross instability lies in the entry section and is independent of the characteristic features of the die exit.

The calculated wall shear stress−apparent shear rate data for the capillary dies with divergent exit lengths of 3, 5, and 8 mm can be shifted manually to superimpose on the data for the capillary die with no divergent exit, as displayed in Figure 2b. This means that the capillary dies that have divergent exits of various lengths can be treated as straight sections of some equivalent length that would give equivalent pressure drops (or equivalent shear stresses) to that of the capillary die with no divergent exit. After manually shifting the data, equivalent capillary lengths of 25.2, 26.8, and 27.0 mm were determined for the capillary dies that had a straight bore die length of 25 mm plus divergent exit lengths of 3, 5, and 8 mm, respectively.

IV. Rheological Characterization

The viscoelastic behavior of the polymer was modeled using an integral K−BKZ constitutive equation that contained the Wagner irreversible damping function.[58] The model parameters were obtained by fitting the linear and nonlinear viscoelastic data in both shear and extension modes. The model was then used in the computational fluid dynamics (CFD) simulations to calculate the principal stress difference (PSD) and velocity

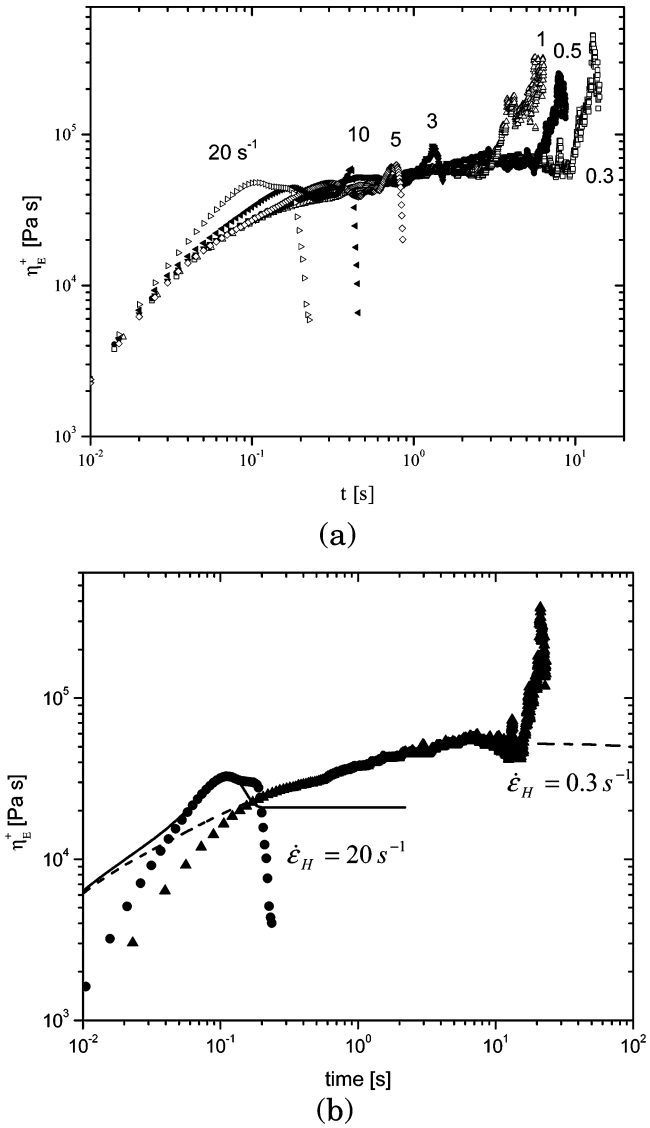

Figure 4. (a) Unshifted transient uniaxial extensional rheology data from SER at 150 °C; (b) shifted transient uniaxial extensional rheology data at 150 °C with Wagner model fit at two different Hencky stretch rates of 0.3 and 20 s^{-1}.

values in the melt that was flowing through the capillary dies and outside the dies.

The total extra-stress tensor in the K−BKZ model, $\sigma(t)$, is given by the following expression:

$$\sigma(t) = -\int_{-\infty}^{t} \sum_{i=1}^{N} \frac{G_i}{\lambda_i} \exp\left(-\frac{t}{\lambda_i}\right)\{\exp[-k\sqrt{\beta I_1 + (1-\beta)I_2 - 3}]\}\boldsymbol{C}^{-1}(t,t')\,dt'$$

where $\boldsymbol{C}^{-1}(t,t')$ is the finger strain tensor; λ_i is the relaxation time of the ith mode; $\boldsymbol{G}_i$ is the strength of the mode; $\boldsymbol{I}_1$ and $\boldsymbol{I}_2$ are, respectively, the first and second invariants of the finger tensor; and $\boldsymbol{k}$ and β are the two model parameters. These are determined by fitting the aforementioned model to shear and extensional data.

Figure 3 shows a superimposition of the dynamic shear and the steady high-shear data. The data shows that the LLDPE melt follows the empirical Cox Merz rule. Figure 3 also shows the prediction of the K−BKZ model for a steady shear flow using

Table 3. Experimental Values and Values Calculated from Simulations for Four Different Flow Rates: (a) Q2 = 9.81 mm³/s, (b) Q3 = 15.5 mm³/s, (c) Q5 = 39.05 mm³/s, and (d) Q9 = 88.31 mm³/s[a]

	sharkskin observed?	ΔP (MPa) experiment	ΔP (MPa) simulated	variation in ΔP (%)	PSD[b] (MPa)	V_0 (mm/s)	V_+ (mm/s)	Δx (mm)	$\dot{\epsilon}$ (s^{-1})	$\dot{T}$ (s^{-1})
(a) Q2 = 9.81 mm³/s										
no divergent exit	no	17.25	18.45	−6.95	1.07	0.2133	1.804	0.004746	335.1	2833.741
(b) Q3 = 15.5 mm³/s										
no divergent exit	yes	21.69	22.86	−5.39	1.37	0.6014	6.790	0.006611	936.1	10568.78
(c) Q5 = 39.05 mm³/s										
no divergent exit	yes	31.05	32.74	5.16	1.65	1.0384	10.2	0.00196	4674	45914
divergent exit−3 mm long	no	31.44	34.09	7.77	0.48	0.0287	0.42	0.01078	36	531
divergent exit−5 mm long	no	32.59	34.36	5.15	0.24	0.0042	0.12	0.009	13	368
divergent exit−8 mm long	no	33.97	34.54	1.65	0.12	0.0019	0.089	0.01524	5.7	268
(d) Q9 = 88.31 mm³/s										
no divergent exit	yes	39.22	37.10	−5.71	1.69	2.4863	24.7	0.00257	8643	85868
divergent exit−3 mm long	yes	40.56	39.23	−3.39	0.70	0.0307	0.81	0.0088	89	2337
divergent exit−5 mm long	no	42.11	39.66	−6.18	0.39	0.0095	0.3	0.00903	32	1016
divergent exit−8 mm long	no	44.79	39.97	−12.07	0.24	0.0042	0.17	0.005881	28	1141

[a] In this table, $\dot{\epsilon}$ and $\dot{T}$ are given by $\dot{\epsilon} = (V_+ - V_0)/\Delta x$ and $\dot{T} \approx \dot{\epsilon}V_+/V_0$. [b] Principal stress difference.

a shear damping coefficient value of $k = 0.2$. A slightly better fit to the experimental data could be obtained for $k = 0.18$. However, we fixed the value of k at 0.2 because some of the CFD simulations at higher flow rates using $k = 0.18$ did not converge, whereas for $k = 0.2$, successful convergence was obtained for all flow rates.

The parameter β was evaluated by fitting the predictions of the K−BKZ model in transient uniaxial extension to the SER data. The transient uniaxial extensional rheology data shown in Figure 4a indicates that, at low stretch rates, there is some evidence of strain hardening, which disappears at higher stretch rates. The strain hardening is probably due to the small amounts of long chain branching produced due to the proprietary constrained geometry single site catalyst used to produce this grade of LLDPE. The SER data, by themselves, are in a raw unshifted format, meaning that the data must be shifted horizontally and vertically to remove the errors that are caused by specimen loading, sample sag, and so on. Figure 4b shows that, at low times, the data do not follow the linear viscoelastic envelope that is predicted by the K−BKZ model, because of errors that are caused by sample sag. However, at longer times, the data do match the predicted viscoelastic envelope well. The K−BKZ model fails to capture the strain hardening at low stretch rates. The value of $\beta = 1$ predicts the data well except for the strain hardening response. We proceed with this value of β, assuming that, in the capillary flow experiments, the stretch rates experienced by the melt near the exit of the capillaries will be much higher than those at which the strain hardening is observed.

V. Numerical Simulations

Numerical simulations of the flow through and out of the capillaries were performed using the commercial CFD package Polyflow. The simulations were performed for two-dimensional, isothermal, axisymmetric, steady-state, and incompressible flows. The entire die geometry that comprised the reservoir prior to the capillary die, the capillary die itself, and the free surface of the swollen extrudate outside the capillary were taken into account for the simulations, as shown in Figure 5. The finite-element formulation in Polyflow uses quadratic interpolation for velocities and linear interpolation for pressure. An adaptive meshing scheme was implemented for simulating the free surface flow after the die exit.

Meshes were constructed for the four capillary dies used in this study, viz., those without a divergent exit and those with

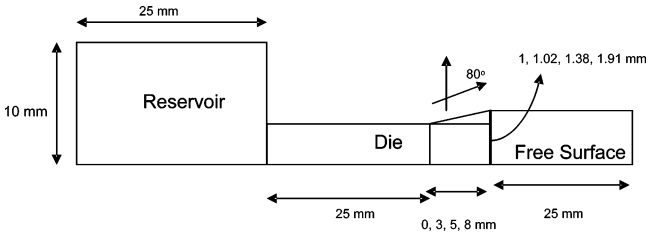

Figure 5. Capillary die geometries that are without a divergent exit and that have divergent exits 3, 5, and 8 mm in length.

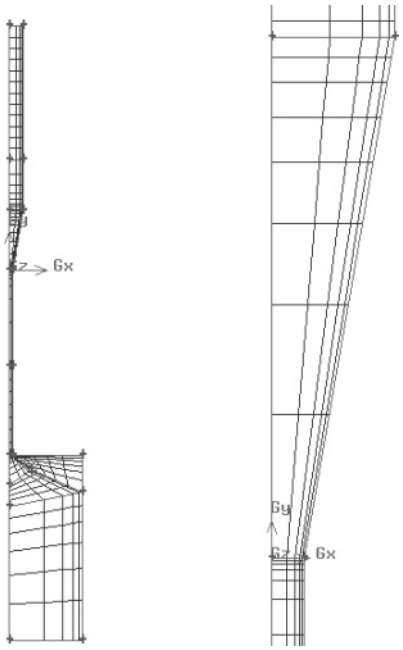

Figure 6. Mesh for the capillary die with a divergent exit 8 mm in length.

divergent exits 3, 5, and 8 mm in length. The angle of the diverging part of the capillary was the same as that used in our experiments, namely, 10°, relative to the vertical (the total angle is 20°). The mesh was made finer near the exit of the capillary die and into the free surface of the swollen extrudate, because the sharkskin singularity is known to occur near this location. Figure 6 shows the initial (before flow) mesh geometry and a close-up of the die exit for a capillary die having divergent length of 8 mm. The number of elements used in each simulation represents the optimum value necessary for a given simulation to run successfully and to give simulated pressure drop values

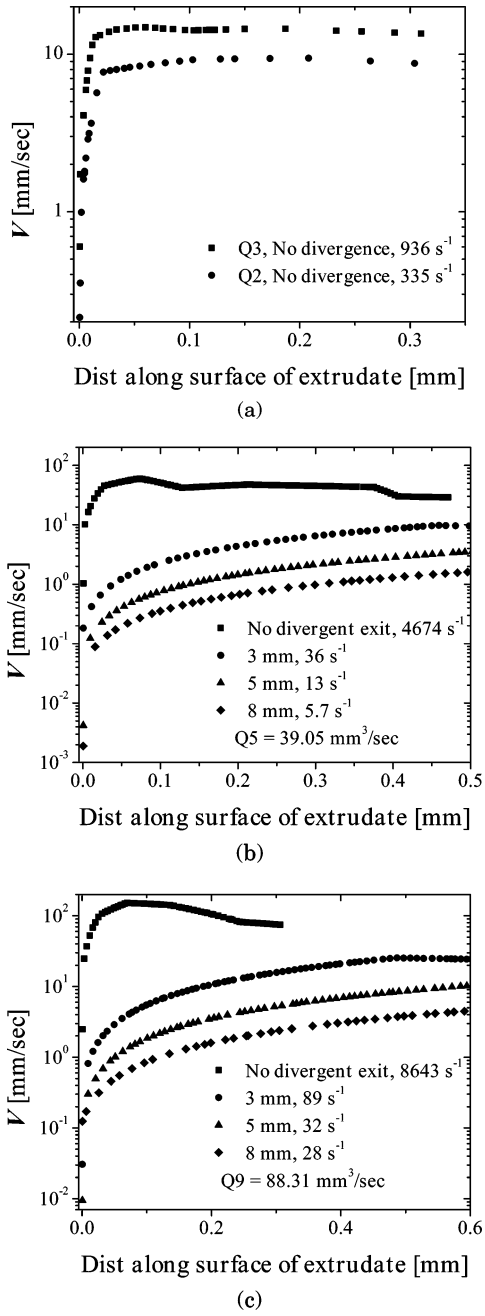

Figure 7. Extension or stretch rate calculations for the surface of the swollen extrudate just leaving the capillary die exit for (a) flow rates Q2 and Q3 and only for dies with no divergence, (b) flow rate Q5 and, (c) flow rate Q9. The values next to the legend are the stretch rates at the die exit.

closest to the observed experimental ones. The value of k and β were taken to be equal to 0.2 and 1, respectively, as explained earlier. No-slip boundary condition was considered at the die wall throughout the die length. Table 3a and b shows that the simulated pressure values are within 10% of the measured values for almost all cases.

As the melt exits the die, a readjustment of the velocity profile causes stretching of material elements close to the extrudate surface, thereby inducing a tensile stress on the melt. Figure 7 displays the velocity of the surface nodes of the swollen extrudate for four different flow rates. Figure 7a−c shows that, for the case of a capillary die with no divergent exit, material elements on the extrudate surface undergo rapid acceleration, which causes the surface of the swelling extrudate to be stretched at very high rates. From the velocity data, we estimate stretch rates to be on the order of 335, 936, 4674, and 8643 s^{-1} for flow rates of 9.81, 15.5, 39.05, and 88.31 mm^3/s, respectively. In stark contrast to the high stretch rates observed in the capillary die that has no divergent exit, the stretch rates for the capillary dies that do have divergent exits are much lower. For example, for a flow rate of 39.05 mm^3/s, the stretch rates are on the order of 36, 13, and 5.7 s^{-1} for the capillary dies with divergent exit lengths of 3, 5, and 8 mm, respectively, as compared to a stretch rate of 4674 s^{-1} for the capillary die that has no divergent exit. This means that, for the capillary dies that have divergent exits, the extrudate surface experiences significantly less-severe stretching deformation.

Figure 8a−d displays the PSD values obtained from simulations for the four different capillary dies at a fixed flow rate (Q5 = 39.05 mm^3/s) at which sharkskin was first observed for the capillary die without a divergent exit. The maximum PSD value for the capillary die without a divergent exit was observed just near the die exit, whereas for the capillary dies with a divergent exit, the maximum PSD values were observed at the point where the diverging section starts and not at the die exit itself. In fact, for these dies, much-lower PSD values were observed in the free surface flow after the die exit and, furthermore, the maximum PSD values anywhere in the flow were lower than those for the capillary die with no divergent exit. While the increase in the total pressure drop with increase in the divergent exit length may be attributed to the greater wall shear effects due to the increased overall length of the die, the trend for the PSD values can be expected from the values of the stretch rates described earlier. The diverging nature of the exit reduces the extensional rates immediately after the die exit and thereby reduces the PSD values.

Table 3 shows the simulated values of the maximum PSD along the free surface immediately after the die exit for the various dies at four different flow rates. The PSD data suggests that, for a die with no divergent exit, when the maximum PSD values just after the die exit exceeded ~1 MPa, then sharkskin was observed on the extrudate surface. This agrees well with the observations of Mackley et al.[38] and Rutgers and Mackley.[42] For the dies that had divergent exits, the maximum PSD values in the free surface immediately after the die exit were determined to be <1 MPa and, correspondingly, no sharkskin was observed, except for the case of the die with a 3-mm divergent exit at a flow rate of 88 mm^3/s, where sharkskin was observed experimentally, even when the maximum PSD in the extrudate just after the die was <1 MPa. We wish to note that the PSD values reported in Table 3 must be treated with caution, because the flow discontinuity at the die exit causes the simulated values to vary significantly with refinement in the mesh density near the die exit. Thus, the values reported in Table 3 are suggestive of the general trends observed in the various dies; the actual values are not emphasized here.

Table 3 also gives the elongational rate ($\dot{\epsilon}$) and the reconfiguration rate ($\dot{T}$) of the polymer melt as it exits the die. The reconfiguration rate is given by

$$\dot{T} \approx \dot{\epsilon} T$$

where $T = V_0/V_+$.[25] V_0 and V_+ are the velocities at two points separated by a distance Δx along a surface stream line. The distance Δx is chosen at a location from the die exit where the velocity profile of the free surface extrudate flow attains plug flow nature. The elongation rate is estimated as

$$\dot{\epsilon} \approx \frac{V_+ - V_0}{\Delta x}$$

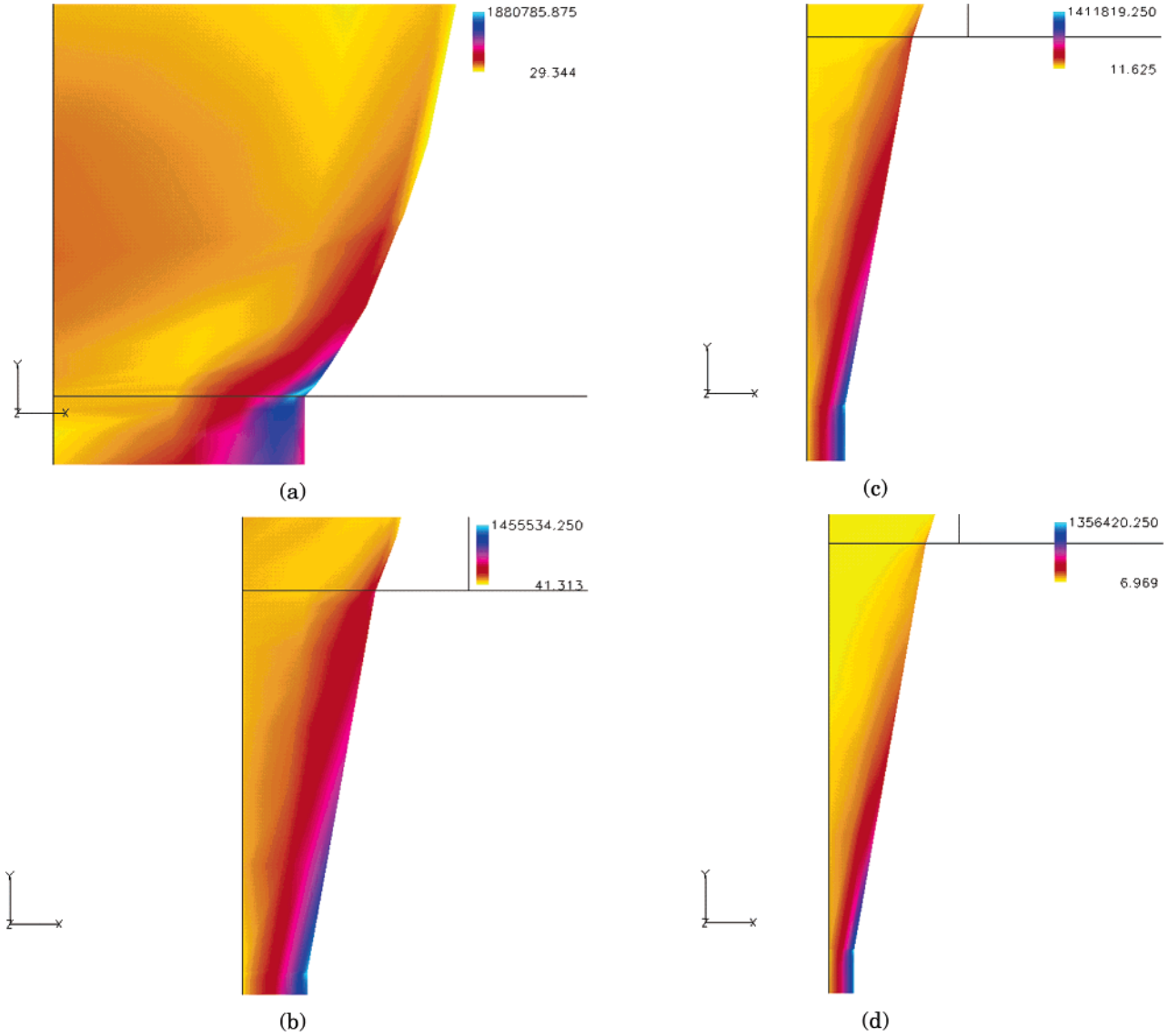

Figure 8. Principal stress difference (PSD) values for a capillary die for a flow rate Q5 with (a) no divergent exit, (b) a 3-mm divergent exit, (c) a 5-mm divergent exit, and (d) an 8-mm divergent exit; the horizontal line on each plot represents the plane of the die exit.

As mentioned previously, Migler et al.[25] argued that neither the elongational rate nor the extensional deformation is solely responsible for the occurrence of sharkskin. They argued that, to estimate a stress level to which material is subjected, one must consider the strain rate as well as the time allowed for stress to build up. As shown in Table 3 for the flow rates Q5 and Q9, $\dot{T}$ as well as the PSD values at the die exit for the die that has no diverging section are at least an order of magnitude greater than the corresponding values for dies that have diverging sections. As shown in Figure 2a for flow rate Q2, sharkskin is not observed for any die, whereas for flow rate Q3, sharkskin is observed for the die that is without a divergent exit. Interestingly, $\dot{T}$ undergoes a sharp jump from 2834 s^{-1} to 10569 s^{-1} as the flow rate changes from Q2 to Q3. Given the approximations involved in the calculations of $\dot{T}$, one may claim that the critical reconfiguration rate to observe sharkskin is ~2800 s^{-1}. For flow rate Q5, the $\dot{T}$ values for all three dies that have diverging sections are smaller than this threshold and no sharkskin was observed using these dies at this flow rate. However, for flow rate Q9, for the die that has a diverging section of 3 mm, $\dot{T} = 2337$ s^{-1}. This is similar to the threshold value and, correspondingly, sharkskin was observed experimentally. For the dies with longer diverging exit sections, the value of reconfiguration rates at this flow rate are much smaller than the aforementioned threshold and no sharkskin was observed.

VI. Conclusion

In this paper, we have studied the effect of die exit curvature on the sharkskin instability. We have experimentally studied the sharkskin behavior of linear low-density polyethylene (LLDPE) through four brass dies with different lengths of diverging section. We observe that, as the length of the diverging section increased, the sharkskin instability was postponed to higher shear rates and the range of shear rates over which sharkskin instability may be observed was decreased. For larger diverging section lengths, the sharkskin instability was observed to be completely absent. As expected, the entry instability started at the same shear rate, irrespective of the diverging section length.

To understand these observations, computational fluid dynamics (CFD) simulations of the flow were performed using a K−BKZ model with a Wagner irreversible damping function

to estimate the stress levels and elongational rates as the polymer exits the die. We observe that, as the length of the diverging section increases, the elongational rate, as well as principal stress difference (PSD) at the die exit, decreases significantly. We observe that the reconfiguration rate criterion, as defined by Migler,[12] may be used to discern the appearance of sharkskin instability.

We believe that the geometrical modification to the dies proposed here can be easily implemented on an industrial scale extrusion operation, to reduce the sharkskin instability.

Literature Cited

(1) Wang, S.-Q. Molecular Transitions and Dynamics at Polymer/wall Interfaces: Origins of Flow Instabilities and Wall Slip. *Adv. Polym. Sci.* **1999**, *138*, 227.

(2) Joshi, Y. M.; Lele, A. K.; Mashelkar R. A. Slipping fluids: A unified transient network model. *J. Non-Newtonian Fluid Mech.* **2000**, *89*, 303.

(3) Kissi, N. El.; Piau, J. M. The Different Capillary Flow Regimes of Entangled Polydimethylsiloxane Polymers: Macroscopic Slip at Wall, Hysteresis and Cork Flow. *J. Non-Newtonian Fluid Mech.* **1999**, *37*, 55.

(4) White, J. L. Critique on Flow Patterns in Polymer Fluids at the Entrance of a Die and Instabilities Leading To Extrudate Distortion. *Appl. Polym. Sci. Symp.* **1973**, *20*, 115.

(5) Garvey, B. S.; Whitlock, M. H.; Freese, J. A. Processing Characteristics of Synthetic Tire Rubber. *Ind. Eng. Chem.* **1942**, *34*, 1309.

(6) Boudreaux, E.; Cuculo, J. A. Polymer Flow Instability: A Review and Analysis. *J. Macromol. Sci.—Rev. Macromol. Chem.* **1977**, *C16*, 39.

(7) Petrie, C. J. S.; Denn, M. M. Instabilities in Polymer Processing. *AIChE J.* **1976**, *22*, 209.

(8) Denn, M. M. Issues in Viscoelastic Fluid Mechanics. *Annu. Rev. Fluid Mech.* **1990**, *22*, 13.

(9) Larson, R. G. Instabilities in Viscoelastic Flows. *Rheol. Acta*. **1992**, *31*, 213.

(10) Graham, M. D. The Sharkskin Instability of Polymer Melt Flows. *Chaos* **1999**, *9*, 154.

(11) Denn, M. M. Extrusion Instabilities and Wall Slip. *Annu. Rev. Fluid Mech.* **2001**, *33*, 265.

(12) Migler, K. B. Sharkskin instability in extrusion. In *Polymer Processing Instabilities*; Migler, K. B., Hatzikiriakos, S. G., Eds.; Marcel Dekker: New York, 2005; p 121.

(13) Benbow, J. J.; Lamb, P. New Aspects of Melt Fracture. *SPE Trans.* **1963**, *3*, 7.

(14) Piau, J. M.; Kissi, N. El.; Tremblay, B. Influence of Upstream Instabilities and Wall Slip on Melt Fracture and Sharkskin Phenomena During Silicones Extrusion Through Orifice Dies. *J. Non-Newtonian Fluid Mech.* **1990**, *34*, 145.

(15) Tordella, J. P. Unstable flow of molten polymers. In *Rheology*; Eirich, F. R., Ed.; Academic Press: New York, 1969; Vol. 5, p 57.

(16) Deeprasertkul, C.; Rosenblatt, C.; Wang, S. Q. Molecular Characters of Sharkskin Phenomenon in Metallocence Linear Low-Density Polyethylenes. *Macromol. Chem. Phys.* **1998**, *199*, 2113.

(17) Pudjijanto, S.; Denn, M. M. A Stable "Island" in the Slip-Stick Region of Linear Low-Density Polyethylene. *J. Rheol.* **1994**, *38*, 1735.

(18) Shaw, M. T.; Wang, L. Sharkskin Melt Fracture: Recent Findings Using Model Geometries. *Proc. Int. Congr. Rheol., 13th* **2000**, (3), 170.

(19) Tapadia, P. S.; Joshi, Y. M.; Lele, A. K.; Mashelkar, R. A. Influence of Stereoregularity on the Wall Slip Phenomenon in Polypropylene. *Macromolecules* **2000**, *33*, 250.

(20) Moynihan, R. H.; Baird, D. G.; Ramanathan, R. Additional Observations on the Surface Melt Fracture Behavior of Linear Low-Density Polyethylene. *J. Non-Newtonian Fluid Mech.* **1990**, *36*, 225.

(21) Hatzikiriakos, S. G.; Dealy, J. M. Effects of Interfacial Conditions on Wall Slip and Sharkskin Melt Fracture of HDPE. *Int. Polym. Process.* **1993**, *8*, 36.

(22) Kissi, N. El.; Leger, L.; Piau, J.-M.; Mezghani, A. Effect Of Surface Properties on Polymer Melt Slip and Extrusion Defects. *J. Non-Newtonian Fluid Mech.* **1994**, *52*, 249.

(23) Kazatchkov, I. B.; Hatzikiriakos, S. G.; Stewart, C. W. Extrudate Distortion in the Capillary/Slit Extrusion of a Molten Polypropylene. *Polym. Eng. Sci.* **1995**, *35*, 1864.

(24) Kissi, N. El.; Piau, J.-M. *Rheology for Polymer Melt Processing*; Elsevier Science: Amsterdam, 1996.

(25) Wang, S. Q.; Drda, P. A.; Y. W. Inn. Exploring Molecular Origins of Sharkskin, Partial Slip, and Slope Change in Flow Curves of Linear Low Density Polyethylene. *J. Rheol.* **1996**, *40*, 875.

(26) Migler, K. B.; Lavalleie, C.; Dillon, M. P.; Woods, S. S.; Gettinger, C. L. Visualizing The Elimination of Sharkskin through Fluoropolymer Additives: Coating and Polymer−Polymer Slippage. *J. Rheol.* **2001**, *45*, 565.

(27) Person, T. J.; Denn, M. M. The Effect of Die Materials and Pressure-Dependent Slip on the Extrusion of Linear Low-Density Polyethylene. *J. Rheol.* **1997**, *41*, 249.

(28) Sornberger, G.; Quantin, J. C.; Fajolle, R.; Vergnes, B.; Agassant, J. F. Experimental Study of The Sharkskin Defect In LLDPE. *J. Non-Newtonian Fluid Mech.* **1987**, *23*, 123.

(29) Nam, S. Mechanism of Fluoroelastomer Processing Aid in Extrusion of LLDPE. *Int. Polym. Process.* **1987**, *1*, 98.

(30) Rudin, A.; Schreiber, H. P.; Duchesne, D. Use of Fluorocarbon Elastomers as Processing Additives for Polyolefins. *Polym. Plast. Technol. Eng.* **1990**, *29*, 199.

(31) Migler, K. B.; Son, Y.; Qiao, F.; Flynn, K. Extensional Deformation, Cohesive Failure, and Boundary Conditions During Sharkskin Melt Fracture. *J. Rheol.* **2002**, *46*, 383.

(32) Kharchenko, S. B.; McGuiggan, P. M.; Migler, K. B. Flow Induced Coating of Fluoropolymer Additives: Development of Frustrated Total Internal Reflection Imaging. *J. Rheol.* **2003**, *47*, 1523.

(33) Kazatchkov, I. B.; Yip, F.; Hatzikiriakos, S. G. The Effect of Boron Nitride on The Rheology and Processing of Polyolefins. *Rheol. Acta* **2000**, *39*, 583.

(34) Muliawan, E. B.; Hatzikiriakos, S. G.; Sentmanat, M. Melt Fracture of Linear PE: A Critical Study in Terms of Their Extensional Behaviour. *Int. Polym. Process.* **2005**, *20*, 60.

(35) Howells, E. R.; Benbow, J. Flow defects in polymer melts. *Trans. Plast. Inst.* **1962**, *30*, 240.

(36) Venet, C.; Vergnes, B. Experimental Characterization of Sharkskin in Polyethylenes. *J. Rheol.* **1997**, *41*, 873.

(37) Constantin, D. LLDPE Melt Rheology: Extensibility and Extrusion Defects. *Polym. Eng. Sci.* **1984**, *24*, 268.

(38) Beaufils, P.; Vergnes, B.; Agassant, J. F. Characterization of the Sharkskin Defect and Its Development with the Flow Conditions. *Int. Polym. Process.* **1989**, *4*, 78.

(39) Kurtz, S. J. Die geometry solutions to sharkskin melt fracture. In *Advances in Rheology*; Mena, B., García-Rejón, A., Rangel-Nafaile, C., Eds.; UNAM Press: Mexico, 1984; p 399.

(40) Ramamurthy, A. V. Wall Slip in Viscous Fluids and Influence of Materials of Construction. *J. Rheol.* **1986**, *30*, 337.

(41) Kalika, D. S.; Denn, M. M. Wall Slip and Extrudate Distortion in Linear Low-Density Polyethylene. *J. Rheol.* **1987**, *31*, 815.

(42) Yang, X.; Ishida H.; Wang, S. Q. Wall Slip and Absence of Interfacial Flow Instabilities in Capillary Flow of Various Polymer Melts. *J. Rheol.* **1998**, *42*, 63.

(43) Mackley, M. R.; Rutgers, R. P. G.; Gilbert, D. G. Surface Instabilities During the Extrusion of Linear Low-Density Polyethylene. *J. Non-Newtonian Fluid Mech.* **1998**, *76*, 281.

(44) Kazatchkov, I. B.; Bohnet, N.; Goyal, S. K.; Hatzikiriakos, S. G. Influence of Molecular Structure on The Rheological and Processing Behavior of Polyethylene Resins. *Polym. Eng. Sci.* **1999**, *39*, 804.

(45) Hatzikiriakos, S. G.; Kazatchkov, I. B.; Vlassopoulos, D. Interfacial Phenomena in the Capillary Extrusion of Metallocene Polyethylenes. *J. Rheol.* **1997**, *41*, 1299.

(46) Rutgers, R. P. G.; Mackley, M. R.; Gilbert, D. Surface instabilities during extrusion of linear low-density polyethylene. In *Dynamics of Complex Fluids*; Adams, M. J., Mashelkar, R. A., Pearson, J. R. A., Rennie, A. R., Eds.; Imperial College Press—The Royal Society: London, 1998; p 30.

(47) Rutgers, R.; Mackley, M. The Correlation of Experimental Surface Extrusion Instabilities with Numerically Predicted Exit Surface Stress Concentrations and Melt Strength for Linear Low-Density Polyethylene. *J. Rheol.* **2000**, *44*, 1319.

(48) Venet, C.; Vergnes, B. Stress Distribution around Capillary Die Exit: An Interpretation of the Onset of Sharkskin Defect. *J. Non-Newtonian Fluid Mech.* **2000**, *93*, 117.

(49) Vinogradov, G. V.; Malkin, A. Y.; Yanovski, Y. G.; Yarlykov, N. V.; Berezhnaya G. V. Viscoelastic Properties and Flow of Narrow Polybutadines and Polyisoprenes. *J. Polym. Sci., Part A-2* **1972**, *10*, 1061.

(50) Cogswell, F. N. Stretching Flow Instabilities at the Exit of Extrusion Dies. *J. Non-Newtonian Fluid Mech.* **1977**, *2*, 37.

(51) Dhori, P. K.; Jeyaseelan, R. S.; Giacomin, A. J.; Slattery, J. C. Common Line Motion III: Implications in Polymer Extrusion. *J. Non-Newtonian Fluid Mech.* **1997**, *71*, 231.

(52) Barone, J. R.; Plucktaveesak, N.; Wang, S. Q. Interfacial Molecular Instability Mechanism for Sharkskin Phenomenon in Capillary Extrusion of Linear Polyethylenes. *J. Rheol.* **1998**, *42*, 813.

(53) Barone, J. R.; Wang, S. Q. Rheo-Optical Observations of Sharkskin Formation in Slit-Die Extrusion. *J. Rheol.* **2001**, *45*, 49.

(54) Bigio, D.; Meillon, M. G.; Kharchenko, S. B.; Morgan, D.; Zhou, H.; Oriani, S. R.; Macosko, C. W.; Migler, K. B. Coating Kinetics of Fluoropolymer Processing Aids for Sharkskin Elimination: The Role of Droplet Size. *J. Non-Newtonian Fluid Mech.* **2005**, *131*, 22.

(55) Joshi, Y. M.; Denn, M. M. Rupture of Entangled Polymeric Liquids in Elongational Flow. *J. Rheol.* **2003**, *47*, 291.

(56) Joshi, Y. M.; Denn, M. M. Rupture of entangled polymeric liquids in elongational flow with dissipation. *J. Rheol.* **2004**, *48*, 591.

(57) Joshi, Y. M.; Denn, M. M. Failure and recovery of entangled polymer melts in elongational flow. In *Rheology Reviews 2004*; Walters, K., Bindings, D., Eds.; British Society of Rheology: Aberystwyth, U.K., 2004; p 1.

(58) Wagner, M. H. Constitutive Analysis of Uniaxial Elongational Flow Data of a Low-Density Polyethylene Melt. *J. Non-Newtonian Fluid Mech.* **1978**, *4*, 39.

Received for review August 8, 2006
Revised manuscript received September 25, 2006
Accepted September 26, 2006

IE0610391